scientific reports

Check for updates

OPEN

# The kinetics of uracil-*N*-glycosylase distribution inside replication foci

Anna Ligasová[1]✉, Ivo Frydrych[1], Barbora Pisklákova[1,2], David Friedecký[2] & Karel Koberna[1]✉

**Mismatched nucleobase uracil is commonly repaired through the base excision repair initiated by DNA uracil glycosylases. The data presented in this study strongly indicate that the nuclear uracil-*N*-glycosylase activity and nuclear protein content in human cell lines is highest in the S phase of the cell cycle and that its distribution kinetics partially reflect the DNA replication activity in replication foci. In this respect, the data demonstrate structural changes of the replication focus related to the uracil-*N*-glycosylase distribution several dozens of minutes before end of its replication. The analysis also showed that very popular synchronisation protocols based on the double thymidine block can result in changes in the UNG2 content and uracil excision rate. In response, we propose a new method for the description of the changes of the content and the activity of different cell components during cell cycle without the necessity to use synchronisation protocols.**

Cells have developed various effective repair mechanisms to eliminate DNA damage and to maintain genome integrity[1]. One of these is base excision repair (BER) that corrects a number of inappropriate and/or modified DNA bases through excision and replacement of a single damaged DNA base e.g.[2]. BER could be initiated by one of the 11 known specific DNA glycosylases recognising and removing the damaged base through the hydrolysis of the *N*-glycosidic bond[3].

Uracil is a typical target of BER[4]. The presence of uracil in DNA may either be the result of incorrect incorporation of dUMP instead of dTMP during DNA synthesis (creation of U:A pairs), or of the deamination of cytosine (creation of U:G pairs). Uracil can be removed from DNA by uracil DNA glycosylases initiating the multistep repair mechanism—BER[5]. In mammalian cells, at least four different monofunctional uracil DNA glycosylases ensure uracil removal from DNA. These are uracil-*N*-glycosylase (UNG), single-strand selective monofunctional uracil-DNA glycosylase 1 (SMUG1), thymine–DNA glycosylase (TDG), and methyl-binding domain 4 protein (MBD4)[3,6]. UNG, SMUG1, and TDG belong to the same protein family[5]. SMUG1 is not cell-cycle-regulated[7] and seems to play an important role in the repair of 5-hydroxymethyl uracil (HmU)[3,5]. TDG has the highest expression in the G1 phase[6] and its most efficiently processed substrates are G:U or G:T mispairs[5,8]. The fourth uracil DNA glycosylase, MBD4, acts on G:U or G:T mispairs[5].

UNG is a dominant type of uracil DNA glycosylase[5] and has an important function both in the post-replicative repair of A:U and G:U pairs[2,3,9]. The gene for human UNG contains 7 exons and encodes both nuclear (UNG2) and mitochondrial (UNG1) forms of the enzyme[10]. The data about UNG2 activity and UNG2 content during cell cycle are not completely consistent, as some authors argue for a high UNG2 expression in the late G1 and the majority of the S phase[2,3,6,9], while others argue for upregulation of UNG2 in G1 phase and its strong downregulation in the S phase[11]. Further, it is taken for granted that UNG2 associates with PCNA and RPA proteins at replication foci, implicating the role of UNG2 in the repair of the misincorporated uracil during DNA synthesis[6,12,13]. On the other hand, it is not clear what is the kinetics of the UNG2 in replication foci, e.g., if UNG2 is present in replication focus for its whole lifetime.

In this study, we measured the uracil excision rate during distinct phases of cell cycle of synchronised HepG2 and HeLa cell. To overcome the impact of synchronisation protocol, we developed and tested an approach based on the FUCCI vector and the direct computation of the mean rate/content of uracil glycosylase activity/UNG2 content in G1, S, and G2/M phases. We also evaluated nuclear UNG activity in cell population with the decreased amount of S-phase cells and its distribution in the distinct cell cycle phases in non-synchronised cells using image cytometry. Finally, we studied kinetics of UNG distribution in replication foci using co-localisation experiments and in silico approach. Our results strongly indicate that both the uracil glycosylase activity and protein content in human cell lines is highest in the S phase of the cell cycle. We also demonstrated that the replication focus undergoes the structural changes related to the UNG distribution before end of its replication.

[1]Institute of Molecular and Translational Medicine, Faculty of Medicine and Dentistry, Palacký University Olomouc, Olomouc, Czech Republic. [2]Laboratory of Inherited Metabolic Disorders, Department of Clinical Chemistry, Palacký University and University Hospital Olomouc, Olomouc, Czech Republic. ✉email: anna.ligasova@upol.cz; karel.koberna@upol.cz

## Results

### Synchronisation of cells by double thymidine block leads to the changes in the uracil excision rate and UNG2 content during cell cycle

Firstly, we analysed the uracil excision rate (UrE rate) in HepG2 cells synchronised by double thymidine (dT) block[4,14–16]. After the release from the dT block, the cells were cultivated for 2, 4, 8, 12, 16, 20, or 24 h. Thereafter, nuclear lysates were prepared. To minimise the impact of the UNG1 protein, we used the method based on the Dounce homogenisation to prepare the nuclear lysates[4]. At the same time points, the cells were labelled with 5-bromo-2'-deoxyuridine (BrdU) for 30 min and the fraction of the cells in G1, S, and G2/M phases was determined by image cytometry. As the UrE rate was related to the overall protein weight in the sample, we similarly transformed the proportions of cells in G1, M, and G2/M phases. G1, M, and G2/M proportions were multiplied by 1, 1.5, and 2, respectively, and the resulting values were divided by their sum (Fig. 1a).

To analyse the UrE rate, we used the method described by Ligasová and colleagues[4]. The method exploits the fluorescence resonance energy transfer (FRET) between a fluorochrome and a quencher within a double-stranded oligonucleotide anchored on magnetic beads (m-sensors). We prepared two types of m-sensors for this purpose. The first type of m-sensor was designed with a single uracil residue within the anchored double-stranded oligonucleotide. The second type of m-sensor, lacking the uracil-thymidine mismatch, served as control (Table 3; chapter Material and Methods, subchapter Measurement of uracil excision rate). Alternatively, either the first type or the second type of m-sensors were added to the wells of the 384-well black plates. Subsequently, the prepared nuclear lysates were added to the wells with m-sensors and the fluorescence signal of 6-FAM was measured using the plate reader.

Although the results could be affected by the presence of UNG1 from mitochondria and/or eventually due to the natural content of UNG1 in the nuclear fraction[17,18], it did not seem to be significant with respect to the possibility to estimate UNG2 activity decrease/increase during the cell cycle in nuclear lysates as the correlation analysis showed that the correlation between UrE rate and UNG2 content is very high (Pearson coefficient = 0.9385, p-value = 0.0006). In addition, no significant correlation between UrE rate and UNG1 content was observed in the tested samples (Supplementary Fig. S1a; Pearson coefficient = -−0.0382, p-value = 0.9284). These data were in accordance with the previously published data[2,6,9,18]. We also analysed if there is a correlation between the UrE rate or UNG2 content and mass fraction of G1, S, or G2/M phases. Although the Pearson coefficient was highest in the case of the S-phase fraction in both cases, the p-value was very high and therefore, the clear decision was not possible (Table 1). Similarly, no significant correlation was observed between UNG1 protein content and mass fraction of G1, S, or G2/M phases (Supplementary Fig. S1b).

From the time course of the UrE rate (Fig. 1b) and UNG2 content (Fig. 1c), it was evident that the first peak of both UrE rate and UNG2 content coincides with the maximal value of S-phase fraction while the minimal value of the UrE rate and UNG2 content coincides with the minimum of S-phase fraction (compare Fig. 1a–c). The high increase of G2/M cells in 8-h sample and the rapid decrease of these cells in the next-time samples indicated that the high fraction of cells undergone cell division between 8 and 12 h. Surprisingly, cells after this division did not exhibit any apparent relation between UrE rate or UNG2 content and the S-phase fraction. Instead, the last sample provided the highest UrE rate and UNG2 content, although it did not exhibit the largest S-phase fraction (Fig. 1). Moreover, synchronisation also resulted in the progressive shortening of the cell cycle as our measurements showed that the doubling time of the non-synchronized HepG2 cells is around 24 h.

We observed even higher correlation between the UrE rate and UNG2 content (Pearson coefficient = 0.9869, p-value < 0.001) when HeLa cells were used (Supplementary Fig. 1d–f). Also in this case, no significant correlation between UrE rate and UNG1 protein content was observed in the tested samples (Supplementary Fig. S1c; Pearson coefficients = 0.5152, p-values = 0.1913). Similarly as in the case of HepG2 cells, the obtained data disabled clear decision about the UrE rate and UNG2 content changes during the cell cycle (Table 2). Although the highest correlation between UrE rate or UNG2 content and the phase mass fraction was also found in the S phase, the p-value was also high. In addition, the highest UrE rate and UNG2 content was also observed in the last sample although this sample did not contain the highest fraction of S-phase cells (Supplementary Fig. 1d–f). Similar to the HepG2 cells, there was relatively high difference between the first cell cycle (up to 12 h) and the second cell cycle after the release from the dT block with respect to the UrE rate and UNG2 content. For example, very similar UrE rate and UNG2 content was observed in the samples from the 2- to 8-h experiments, although high decrease of S-phase fraction and high increase of G2/M-phase fraction was observed in the 8-h experiment compared to the 2- and 4-h experiments. The highest UrE rate and UNG2 content was observed in the last, 24-h, experiment although this sample did not contain the largest S-phase cell fraction. Concerning UNG1, no significant correlation was observed between UNG1 content and mass fraction of G1, S, or G2/M phases (Supplementary Fig. S1b).

Although the obtained data did not allow the clear conclusions about the changes of the UrE rate and UNG2 content during cell cycle, they showed that there is a difference between cells before and after the first division after the removal from the dT block. It indicates that the dT block can result into relatively large changes of cellular metabolic pathways connected with the uracil repair.

In this respect, we did not observe similar effect in the case of the analysis of the content and the activity of cytidine deaminase (CDD) both in HepG2 and HeLa cells (Supplementary Fig. 2). This enzyme contributes to the elevation of the deoxyuridine pool by deamination of cytidine and deoxycytidine[19]. Therefore, it seems that the dT block has a specific impact on the uracil repair, but, not on the overall pathway of uracil metabolism.

To overcome this impact, we tested a synchronisation protocol based on the CDK1 inhibitor (RO-3306 inhibitor)[20,21] to block the cells in G2/M phase. However, we did not obtain satisfactory synchrony of HeLa cells in G2/M phase. Although incubation of cells with RO-3306 led to the increased number of G2-cells (Supplementary Fig. 3a) and to the slightly decreased UrE rate (Supplementary Fig. 3b), it did not lead to the decrease of the number of replicating cells (Supplementary Fig. 3a).

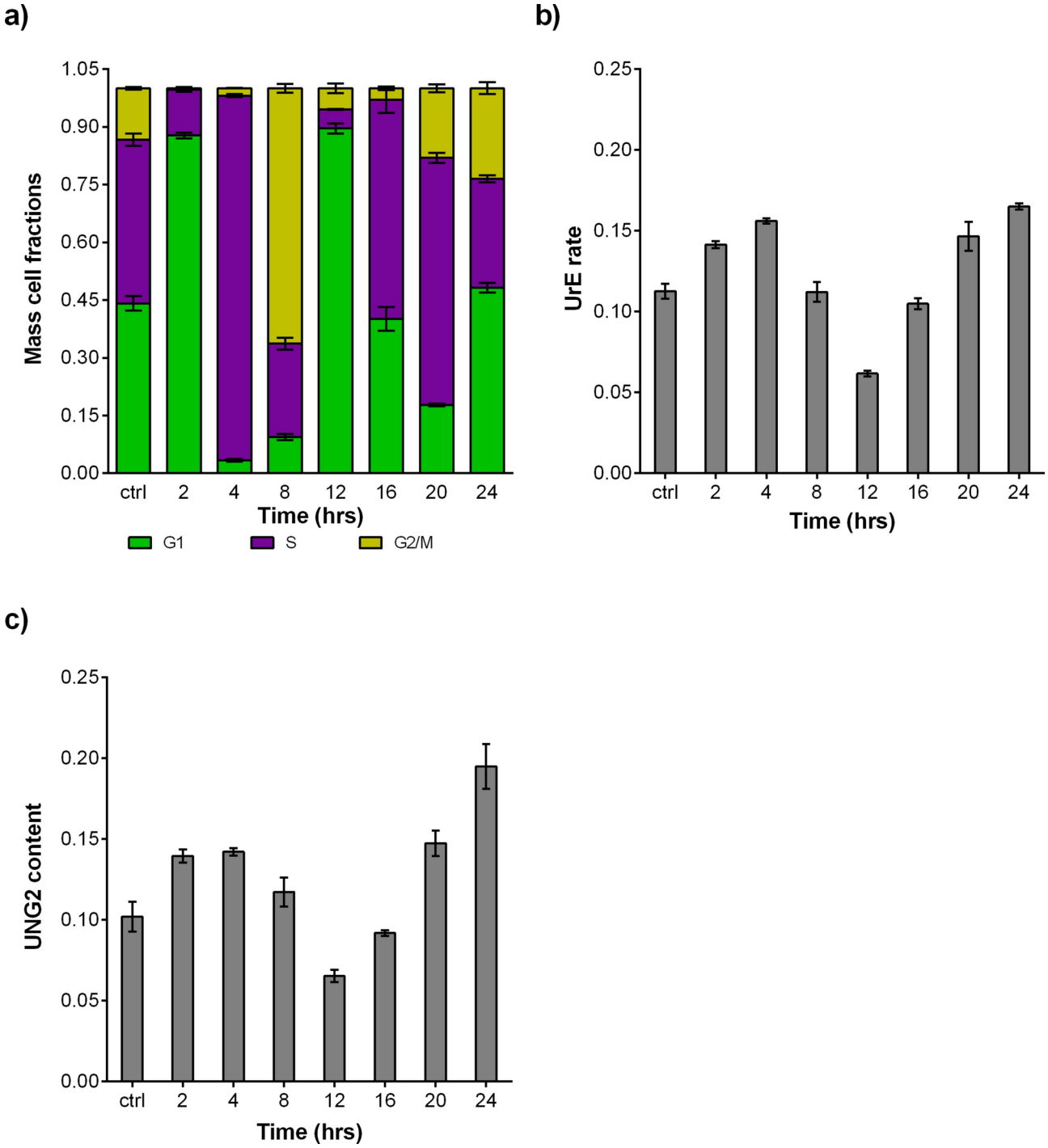


**Fig. 1**. Uracil excision rate and UNG2 content during cell cycle of HepG2 cells. (**a**) Analysis of the cell cycle of HepG2 cells at various time points after the release from the dT block. The estimated mass fraction of cells in G1, S, and G2/M phases was determined in the indicated times after the release from the dT block by image cytometry using DAPI and BrdU labelling. (**b**) Analysis of UrE rate in nuclear lysates of HepG2 cells at the same time points as in (**a**) after the release from the dT block. The data are shown as the mean ± SD. (**c**) Analysis of the UNG2 content in nuclear lysates of HepG2 cells determined by western blot at the same time points as in (**a**) and (**b**) after the release from the dT block. The mean intensities of the bands were measured and plotted. The data are shown as the mean ± SD.

## The uracil excision rate in nuclear lysates of non-synchronised HeLa FUCCI cells is highest in S phase

As the synchronisation protocol resulted in various effects on cell metabolism including the shortening of the cell cycle and this effect can be also cell line-dependent[22], we developed and tested the system based on the

| UrE rate | Pearson coefficient | p-value |
|---|---|---|
| G1 | −0.4247 | 0.2942 |
| S | 0.4709 | 0.2390 |
| G2/M | −0.0064 | 0.9879 |
| **UNG2 content** | **Pearson coefficient** | **p-value** |
| G1 | −0.2923 | 0.4824 |
| S | 0.2206 | 0.5996 |
| G2/M | 0.1375 | 0.7455 |

**Table 1**. Correlation analysis of the UrE rate/UNG2 content and the mass fraction of particular cell cycle phases in HepG2 cells.

| UrE rate | Pearson coefficient | p-value |
|---|---|---|
| G1 | −0.6094 | 0.1087 |
| S | 0. 4991 | 0.2080 |
| G2/M | 0.1771 | 0.6749 |
| **UNG2 content** | **Pearson coefficient** | **p-value** |
| G1 | −0.6816 | 0.0627 |
| S | 0.5023 | 0.2046 |
| G2/M | 0.2926 | 0.4818 |

**Table 2**. Correlation analysis of the UrE rate/UNG2 content and the mass fraction of particular cell cycle phases in HeLa cells.

FUCCI (Fluorescent Ubiquitination-based Cell Cycle Indicator) construct, fluorescence activated cell sorting (FACS), and computation approach to measure UrE rate during the cell cycle (Fig. 2a). The FUCCI construct is a set of genetically encoded fluorescent probes which uses two proteins participating in the replication licensing—geminin and Cdt1 protein[23]. Their amount is cell-cycle-dependent. A fragment of Cdt1 is linked to the Kusabira-Orange 2 fluorescent protein and is used to label cells in the G1 phase; a fragment of geminin is linked to Azami-Green 1 fluorescent protein and is used to label S/G2/M cells. As the highest amount of Cdt1 is in the G1 phase and decreases during the S phase, and the highest amount of geminin is in the S and G2 phases and decreases in the M phase, this technology allows FACS separation of cells into different cell fractions enriched in red-labelled G1 cells, orange-labelled cells at the beginning of the S phase, and green-labelled cells in the S/G2/M phase[23–28].

We sorted the HeLa FUCCI cells into three different samples with the different expression of fluorescent proteins. Simultaneously, we sorted the HeLa FUCCI cells labelled with 10 μM 5-ethynyl-2'-deoxyuridine (EdU). This sample served to determine the proportion of particular cell-cycle phases (Fig. 2b) and the mass cell fraction of these phases (Fig. 2c). UrE rate analysis showed the elevated signal in the second sample (Fig. 2d). Next, we create a system of three equations containing sum of fractions of cells in G1, S, and G2/M phases on one side and the measured UrE rate on the second side (Supplementary Table 1). Example Eqs. (1–3) are listed below:

$$0.65 \times \mathrm{G1rate} + 0.26 \times \mathrm{S\ rate} + 0.09 \times \mathrm{G2/M\ rate} = 0.3128 \quad (1)$$

$$0.30 \times \mathrm{G1\ rate} + 0.61 \times \mathrm{Srate} + 0.09 \times \mathrm{G2/Mrate} = 0.3603 \quad (2)$$

$$0.10 \times \mathrm{G1\ rate} + 0.58 \times \mathrm{Srate} + 0.32 \times \mathrm{G2/Mrate} = 0.3269 \quad (3)$$

The calculated equation solutions showed that the S-phase cells exhibited the highest level of UrE rate (Fig. 2e, p-value = 0.01; Mann–Whitney test). These results indicated that a computational approach based on the cells expressing the FUCCI construct can be a useful alternative for the analysis of the activity of various cell components during the cell cycle. Although this approach does not allow for discrimination between the different times in the distinct phase, it provides possibility to address the differences between cell cycle phases without the necessity to use synchronisation protocol. It speeds up the whole analysis and minimises the impact on the cell metabolism.

## Immunocytochemical detection of nuclear UNG protein provides results compatible with the data from HeLa-FUCCI cell lysates

Next, we used immunocytochemical detection of nuclear UNG protein using the specific antibody and image cytometry to evaluate the differences between cells in different phases of cell cycle. For this purpose, HepG2, HeLa, hTERT RPE-1, and IMR-90 cells were incubated with EdU for 30 min, fixed, and EdU, DNA, and nuclear UNG protein were detected using azido-fluorochrome, DAPI, and fluorescently labelled specific antibody, respectively. The signal was acquired by fluorescence microscope, nuclei were identified using ilastik software,

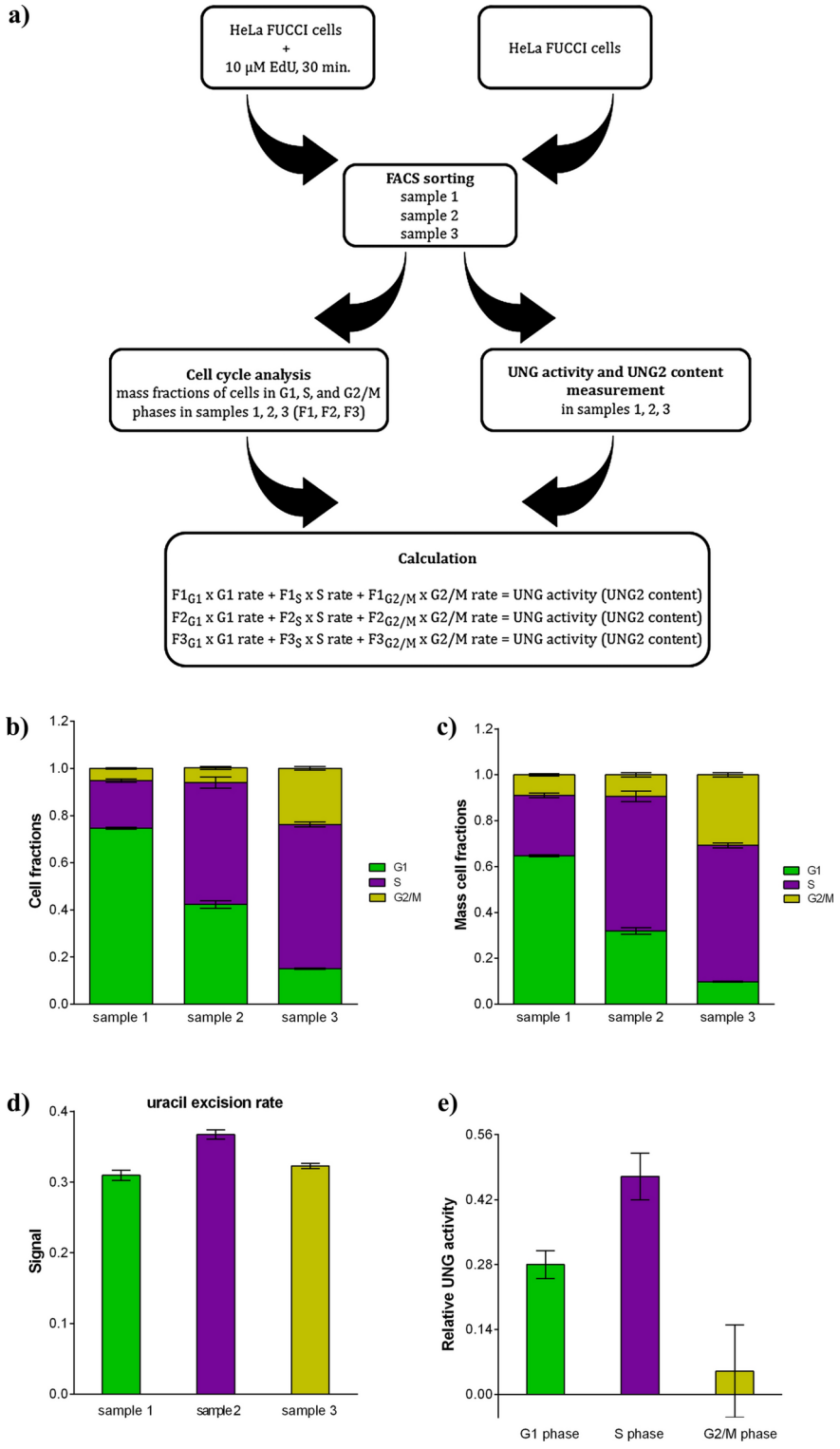


**Fig. 2**. Uracil excision rate during cell cycle of HeLa FUCCI cells. (**a**) Simplified scheme of the developed method. (**b**) Analysis of the cell cycle of HeLa FUCCI cells. The fractions of cells in the G1, S, and G2/M phases were determined by image cytometry and DAPI and EdU labelling. (**c**) Estimated mass fraction of cells in particular phases of the cell cycle calculated from data in (**b**). Each cell fraction in each sample was multiplied by the growth coefficient and divided by the sum of these values in every sample. (**d**) Analysis of the UrE rate in nuclear lysates of HeLa FUCCI cells. Cells were sorted by FACS into three samples using the same FACS parameters as in the case of cells labelled with EdU. The data are shown as the mean ± SD. (**e**) The results of the calculation of UrE rate in HeLa FUCCI cells in G1, S, and G2/M phases using the system of three equations. The data are shown as the mean ± SD.

and the nuclear signal was measured using CellProfiler software. For the identification of G1, S, and G2/M cells, scripts based on Python, Pandas, Numpy, and SciPy libraries were used. To assess the statistical significance of the elevated nuclear UNG signal observed during the S phase, we performed a Mann–Whitney test comparing the S-phase signal to the G1- and G2/M-phase signals (Fig. 3). The significant p-values (< 0.001) support the hypothesis that the increased S-phase signal could be a general phenomenon in cells.

These data argue for the highest nuclear UNG protein content in S-phase cells irrespectively of the cell line used. If the data from HeLa FUCCI cells are included, there is approximately only 0.004 chance that this is a product of the random choice.

In order to address this issue in cells specifically during the S phase, the S-phase cells were selected using EdU and DNA signals first. Nuclear EdU signal was divided into 10 intervals of the same size or in the case of IMR-90 cells into 7 intervals and the cells belonging to the distinct intervals were separated into 10 or 7 groups. Then, the mean value of nuclear EdU signal and nuclear UNG signal was calculated in every group and plotted (Fig. 4a, c, e, g). This approach results in the decrease of the points and therefore provides more clearly arranged plots. Alternatively, the non-processed nuclear EdU and UNG signals were used to create the scatter plots (Figs. 4b, d, f, h). The Pearson coefficient and the p-value were calculated for every plot (Fig. 4). The clear positive correlation between the nuclear EdU and UNG signal was observed independently of the cell line or approach used. It indicates that generally cells exhibiting higher nuclear EdU signal also exhibit higher nuclear UNG signal and vice versa. Our analysis also indicates cell-type specificity of the correlation. The Pearson coefficient for the non-

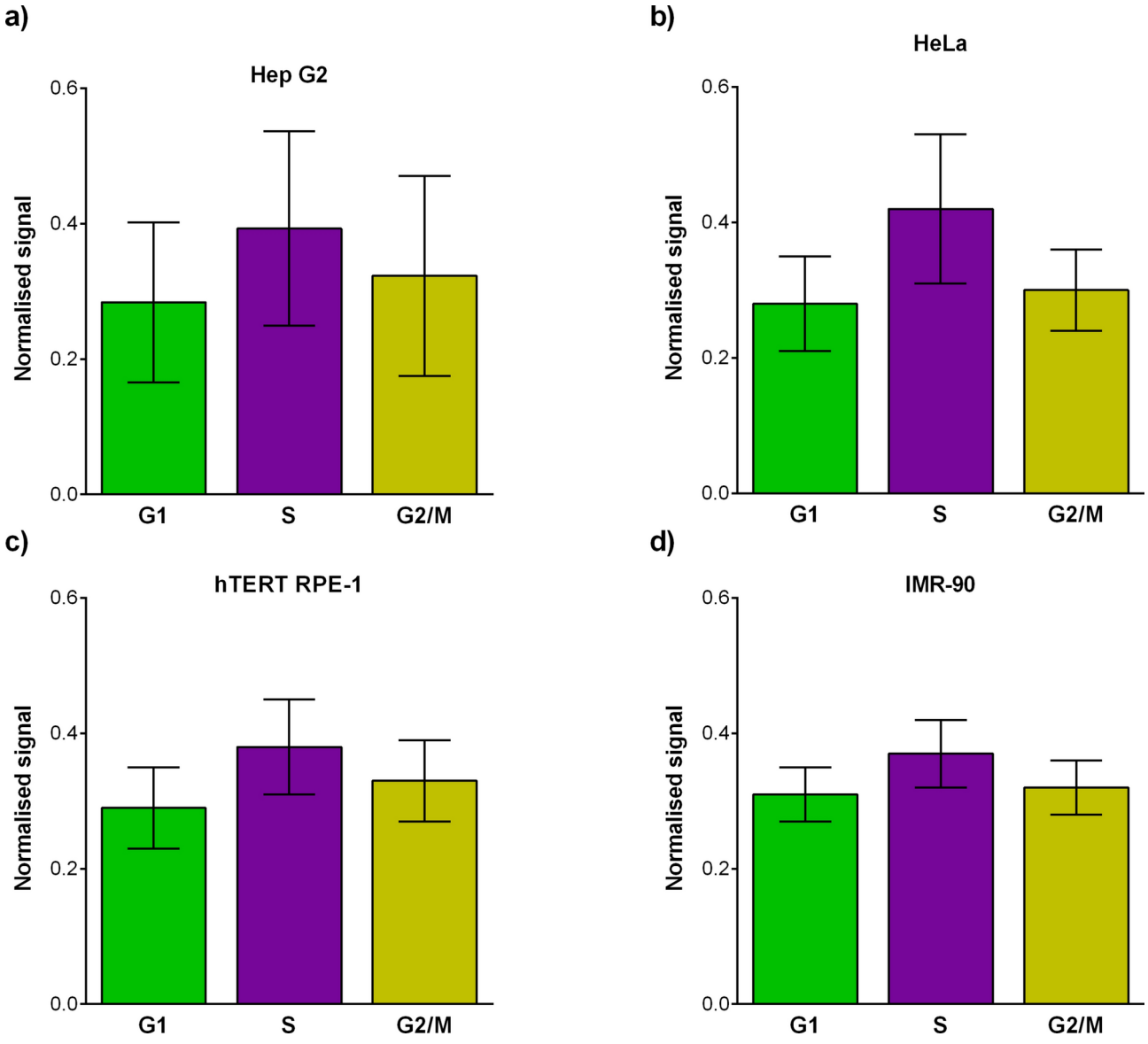


**Fig. 3**. Analysis of the nuclear UNG signal in particular cell cycle phases in various cell lines. Analysis of the nuclear UNG signal in particular cell cycle phases in HepG2 (**a**), HeLa (**b**), hTERT RPE-1 (**c**), and IMR-90 (**d**) cells is shown.

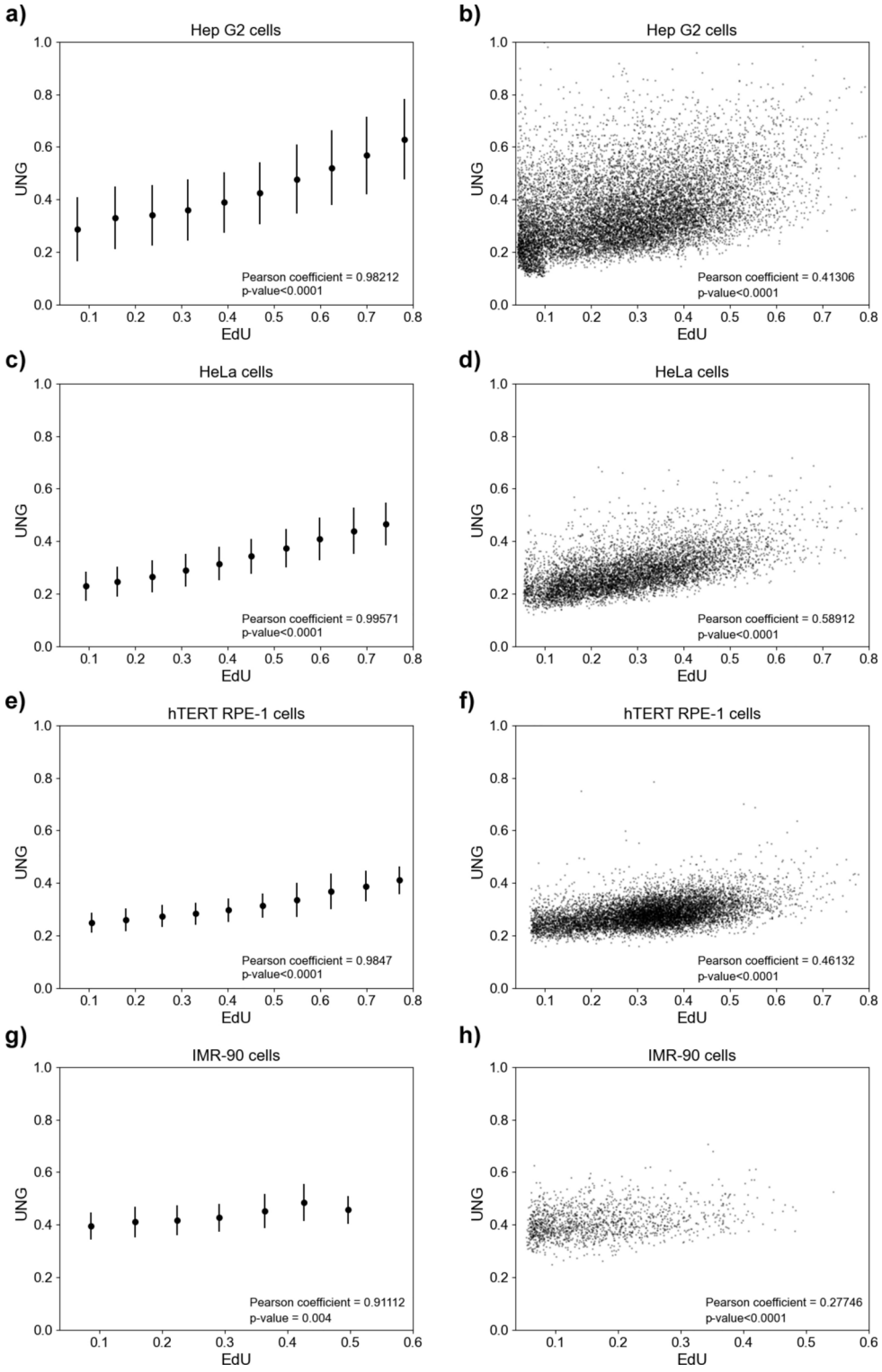


**Fig. 4**. Correlation analysis of the mutual distribution of nuclear UNG protein and replicating cells (EdU signal). (**a**), (**c**), (**e**), and (**g**) Correlation analysis based on the division of EdU signal into 10 intervals (7 intervals in the case of IMR-90 cells) of the same size. The mean values of nuclear EdU signal and UNG signal were calculated in every group and plotted. (**b**), (**d**), (**f**), and (**h**) The scatter plots of the non-processed nuclear EdU and UNG signals.

processed signals was significantly lower (p-value < 0.001) in IMR-90 cells compared to all other tested cell lines (Mann–Whitney test). This suggests that the observed association between nuclear EdU and UNG levels might be more pronounced in specific cell types. The script used for calculating the p-value for comparing the Pearson coefficient with the Fisher Z-Transformation is available at https://github.com/psinger/CorrelationStats/blob/master/corrstats.py.

## Decrease of replication activity using contact inhibition lead to decrease of nuclear UrE rate

As the tested synchronisation protocols resulted in the changes of cellular metabolism, we decreased the number of replicating cells in three non-cancer cell lines (WI-38, MRC-5, and hTERT.

RPE-1 cells) by contact inhibition to test if this decrease will be accompanied by the decrease of UrE rate. Contact inhibition is a process of arresting cell growth when cells come in contact with each other. As a result, normal cells stop proliferation when they form a monolayer in a culture dish[29]. In all cases, we found profound decrease of the amount of replicating cells comparing to the control samples (Supplementary Fig. 4). This decrease was accompanied by the decrease of UrE rate (Fig. 5a) (p-value < 0.001, p-value = 0.035, p-value = 0.015 for WI-38, MRC-5, and hTERT RPE-1, respectively; Mann–Whitney test).

## Replicative senescence results in substantial decrease of nuclear uracil excision rate

As the contact inhibition cannot be applied to decrease the fraction of replicating cells in cancer cell lines, we tried to decrease the fraction of replicating cells using the treatment of cancer cells by the known inducer of senescence, BrdU[30].

As 5-bromouracil (BrU) could interfere with uracil excision, we first tested the possibility that BrU is excised from DNA by the similar pathway as uracil. We used the similar probe as described in Material and Methods (Table 3; chapter Material and Methods, subchapter Measurement of uracil excision rate) containing BrU instead

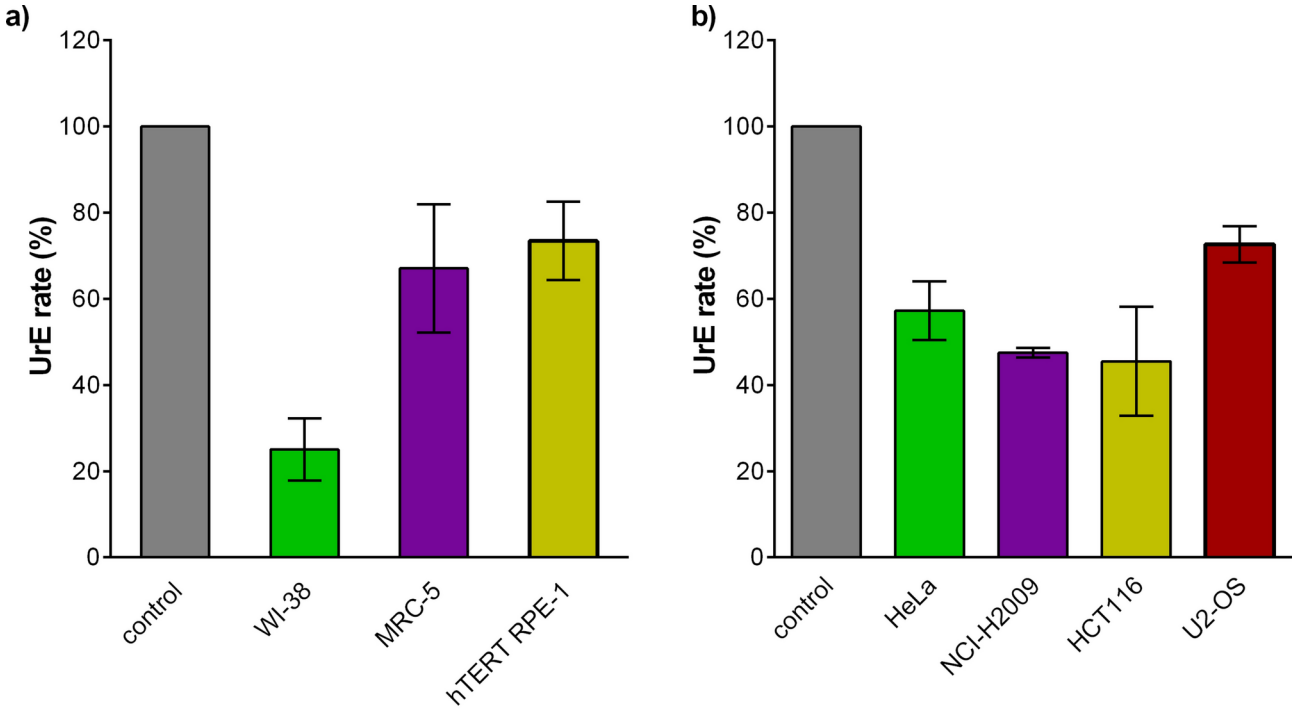


| | p-value |
|---|---|
| WI-38 | <0.001 |
| MRC-5 | 0.035 |
| hTERT RPE-1 | 0.015 |

| | p-value |
|---|---|
| NCI-H2009 | <0.001 |
| HCT-116 | <0.0036 |
| U2-OS | <0.001 |
| HeLa | <0.001 |

**Fig. 5**. Analysis of uracil excision rate in nuclear lysates of contact-inhibited cells and in senescent cells. (**a**) Results of the analysis of the UrE rate in nuclear lysates of three contact-inhibited non-cancer cells. The UrE rate was normalised to the UrE rate in the control, non-treated cells (grown to 50–70% confluency) equal to 100%. The data are shown as the mean ± SD. (**b**) Results of the analysis of UrE rate in nuclear lysates of four cancer cell lines after induction of senescence by BrdU. The UrE was normalised to the UrE rate in the control, non-treated cells equal to 100%. The data are shown as the mean ± SD.

of uracil. In contrast to the probe with uracil, we did not observe excision of BrU from the probe in nuclear lysates (Supplementary Fig. 5). It indicated that BrU is not efficiently removed from the nuclear DNA by UNG and therefore, its incorporation does not directly interfere with uracil excision. Then, we defined conditions resulting in the senescence induction in particular cell lines as too high BrdU concentration and/or too long treatment can result in apoptosis while too low BrdU concentration and/or too short treatment do not result in the senescence induction.

Senescence induction was controlled by the incorporation of EdU[31,32], senescence-associated β-galactosidase (SA-gal) assay, and DAPI. In this respect, the 6-day incubation of HeLa cells with 60 μM BrdU resulted in the decrease of the fraction of EdU-positive cells from 41.8 ± 5.7% to 14.8 ± 4.1% (Supplementary Fig. 6a). Similar decrease of the fraction of replicated cells was observed also in the case of the 8-day incubation of NCI-H2009 cells with 100 μM BrdU (from 41.8 ± 0.5% to 22.4 ± 0.1%; Supplementary Fig. 6a). In the case of 4-day incubation of HCT-116 and U2-OS with 100 μM BrdU, the decrease of replicating cells was as follows: from 58.2 ± 1% to 7.6 ± 0.9% and from 52.8 ± 0.8% to 25.4 ± 0.9%, respectively (Supplementary Fig. 6a). The decrease of the fractions of replicating cells was also accompanied by the appearance of SA-gal positive cells (example in Supplementary Fig. 6b), change in cells' morphology, and the appearance of senescence-associated heterochromatin foci (SAHF) detected by DAPI labelling.

The analysis of UrE rate in nuclear lysates of senescent cells showed that the UrE rate decreased in all tested cells after BrdU treatment (Fig. 5b). The p-values for NCI-H2009, HCT-116, U2-OS, and HeLa cells were < 0.001; < 0.0036, < 0.001, and < 0.001, respectively (Mann–Whitney test).

## The kinetics of UNG signal distribution in replication foci positively correlates with the replication activity

The presence of UNG2 protein was previously documented in replication foci of HaCaT cells[13]. Other studies also showed that the UNG2 co-localizes with the PCNA protein in HeLa and U2-OS cells[9,33]. On the other hand, the kinetics of this distribution with respect to replication foci was never directly addressed. To study this issue, we incubated HeLa cells with EdU for 30 min. Then we alternatively incubated cells for 0, 30, 60, 90, and 120 min in EdU-free medium followed by an additional 30 min in the culture medium with BrdU. The cells were fixed and EdU and BrdU were detected by fluorescent probes (for the simplified scheme see Supplementary Fig. S7). In parallel experiments, HeLa cells were labelled with EdU for 30 min and incubated in EdU-free medium for 0, 30, 60, 90, and 120 min. Cells were fixed and EdU and nuclear UNG signals were detected by fluorescent probes.

Images were acquired by fluorescence microscope and evaluated using SIMCIM tools software. As the fluorescence pattern provided by UNG antibody did not allow with some exception the quick and clear discrimination of the presence of UNG protein in the EdU-labelled domains (Fig. 6), we used several methods based on the systematic determination of the Pearson coefficient or overlap between EdU and BrdU or EdU and UNG signals.

Around 50 nuclei exhibiting EdU signal from 10–20 images were evaluated in every time point of the experiment (0, 30, 60, 90, and 120 min). Two squared areas (working frames, 60 × 60 pixels) containing the highest EdU signal were selected in every nuclei first. Then, two smaller areas (selection frames, 25 × 25 pixels) exhibiting the highest variance of EdU signal were selected in these larger areas. For both selection processes, automatic selection tool (SIMCIM tools software) was used. The position of areas was saved and later used for the three different batch analysis to follow the kinetics of the mutual distribution of EdU and BrdU signals or EdU and nuclear UNG signals.

The first analysis was based on the computation of the Pearson coefficient in the concatenated selections with the normalized EdU and BrdU or EdU and nuclear UNG signals. The signal was normalized in the range of 0 and 1. In the case of EdU and BrdU signals, the analysis shows that the Pearson coefficient gradually decreases with the prolongation of the chase between EdU and BrdU pulses (p-value < 0.001; the script used for calculation was based on Fisher Z-Transformation; Fig. 7a, Supplementary Fig. 8a). The complete separation of both signals (Pearson coefficient close to 0) was observed in the two-hour chase (Fig. 7a). It indicates that the maximal replication focus lifetime in HeLa cells is around 2 h. The nuclear EdU and UNG signal analysis showed that the Pearson coefficient decreases up to 1.5-h chase and then slightly increase (Fig. 7b, Supplementary Fig. 8b). Despite that it was evident that the Pearson coefficients from EdU/BrdU and EdU/UNG analysis highly correlated (Pearson coefficient = 0.92178, p-value = 0.026). For the chase times from 0 to 1.5 h, the correlation was even higher (Pearson coefficient = 0.99226, p-value = 0.008). It strongly indicates that nuclear UNG distribution perfectly matches the replication foci kinetics in this time window. It also indicates that this decrease is finished before the complete separation of EdU and BrdU signals.

| Name | 5′ modification | 5′→3′ direction | 3′ modification |
|---|---|---|---|
| Anchoring oligonucleotide | | | |
| $B_{30FAM}$ | 6-FAM | CGT GAA TTC TTA AAC CGC GAC GAC ATC CGC | Biotin |
| Complementary oligonucleotides | | | |
| $C_{TQ}$ | – | TTT AAG AA**T** TCA CG | BHQ1[a] |
| $C_{UQ}$ | – | TTT AAG AA**U** TCA CG | BHQ1[a] |
| $C_{BrQ}$ | – | TTT AAG AA**Br** TCA CG | BHQ1[a] |

**Table 3**. List of used oligonucleotides. [a]BHQ1, quencher suitable for fluorochromes emitting in the wavelength range 480–580 nm, absorption maximum is 534 nm.

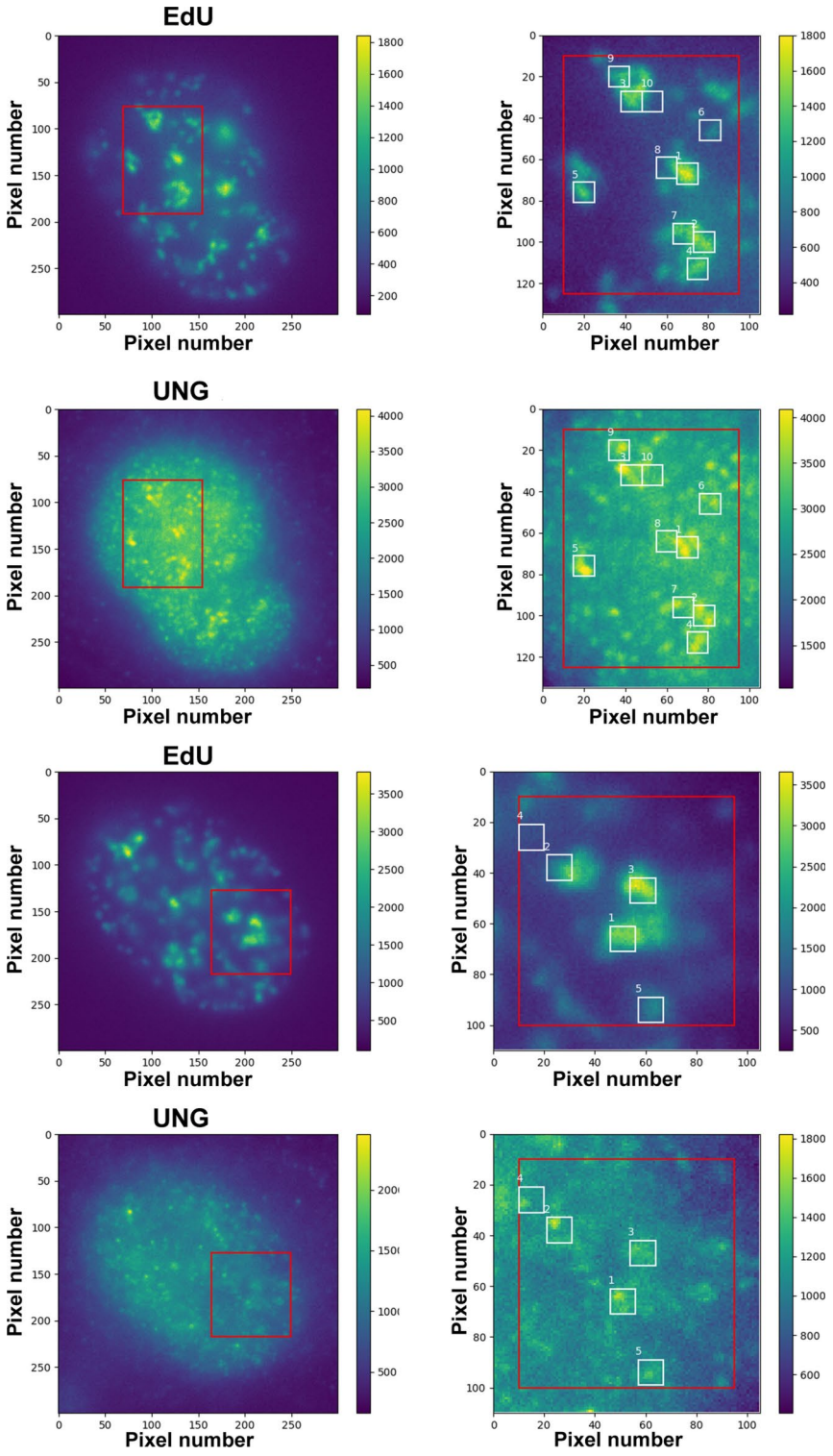


**Fig. 6**. The distribution of nuclear UNG signal with respect to the replication (EdU) signal. Two examples of the distribution of nuclear UNG signal with respect to the replication (EdU) signal in HeLa cells are shown. Although the upper set of four images provided relatively well-differentiated UNG signal resembling the distribution of EdU-labelled replication foci, no such distribution of the nuclear UNG signal was observed in the lower set of images. The fluorescence pattern in the second image set was much more frequent than the fluorescence pattern in the first image set. The numbered white boxes represent areas with the highest nuclear UNG signals (10 × 10 pixels) in the red frame. The box numbers reflect the signal intensity. The highest signal is in a box with the number one. Pixel size: 1 pixel = 63.924 × 63.924 nm.

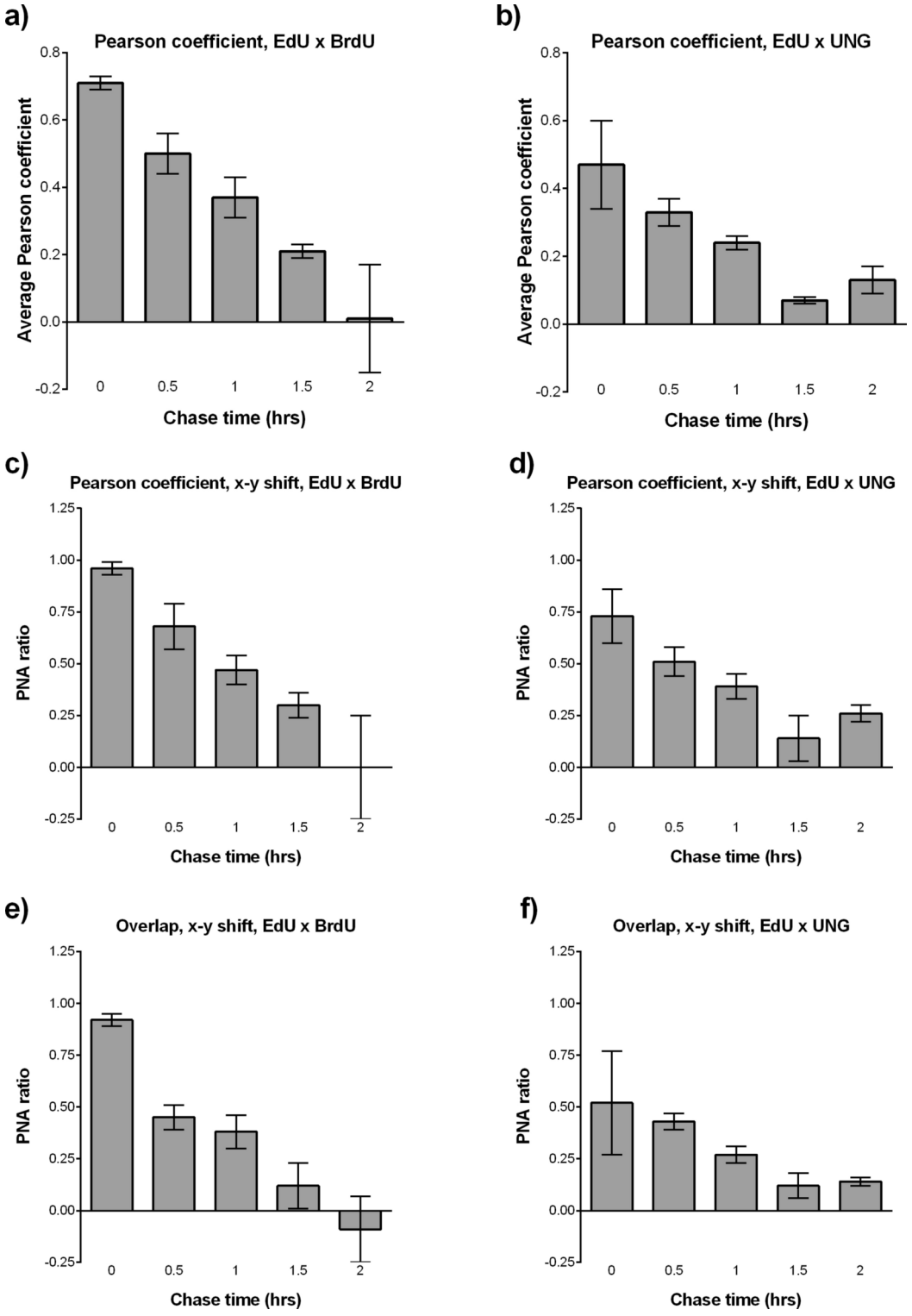


**Fig. 7**. Pearson coefficients in the concatenated selections and PNA rations calculated from the x–y shift analysis using either Pearson coefficient or overlap. (**a**, **b**) Pearson coefficients computed from the selected areas for EdU signal and BrdU (**a**) or nuclear UNG (**b**) signal after 0-, 0.5-, 1-, 1.5-, and 2-h chase. Pearson coefficient was calculated after concatenation of areas with the normalized signal (from 0 to 1). (**c**–**f**) PNA ratios computed from the selected areas for EdU signal and BrdU (**c**, **e**) or nuclear UNG (**d**, **f**) signal after 0-, 0.5-, 1-, 1.5-, and 2-h chase.

To address the impact of the random co-localization on the results, we applied two additional methods based on either the x–y shift analysis using Pearson coefficient or the overlap in the EdU channel and BrdU or UNG channels (Fig. 7c-f). In both cases, the selection frame around every selection was gradually shifted pixel by pixel from the left upper corner to the right lower corner of the working frame in the BrdU or UNG images. The Pearson coefficient or overlap was calculated for the BrdU or UNG signal at every such position and for the EdU signal in the non-shifted original position (Supplementary Fig. 7). We determined the number of shifted frames exhibiting either a higher or lower Pearson coefficient or overlap compared to the Pearson coefficient or overlap observed in the original, non-shifted selection frames. The analysis provided three categories of data: positively correlated selection frames, negatively correlated selection frames, and non-correlated selection frames. Positively correlated selection frames were those which provide higher Pearson coefficient or overlap then 95% of the shifted areas. Negatively correlated areas were those which provide lower Pearson coefficient or overlap then 95% of the shifted areas. The remaining areas were considered non-correlated. To get only one value from these analyses, the PNA ratio was calculated. It is equal to the ratio of the difference between the number of positive (P) and negative (N) selection frames and sum of all selection frames (A). Similarly as Pearson coefficient, the PNA ratio has the value between -1 and 1 and its interpretation is similar as in the case of Pearson coefficient. Both methods provided similar results as analysis of Pearson coefficient (compare Fig. 7a–b and c–f). Pearson coefficients and p-values for EdU/BrdU and EdU/UNG results were equal to 0.8850 and 0.0460, respectively for the analysis based on x–y shift using Pearson coefficient and 0.9298 and 0.0221, respectively for the analysis based on x–y shift using overlap. These high values further confirmed very high spatial correlation between replication foci and UNG protein.

All these data also indicated that the UNG content decreases progressively in the replication focus before completion of its replication. To address this issue, we simulated both experiments (EdU × BrdU) and (EdU × UNG) using two Python scripts. At first, we generated 1,000 replication foci randomly distributed between 0 and 10 h. The lifespan of every replication focus was generated using normal distribution with the mean value from 0.5 to 4 h and the standard deviation from 0 to 1 h using 0.1-h step. Both simulations started at 2 h by EdU pulse. The chase length was chosen from 0- to 2-h interval using a 30-min step. We used several methods to analyse the best match between the simulated and experimental datasets. They were (1) the calculation of Euclidean distance; (2) the calculation of the Dynamic Time Warping distance; and (3) the distance calculated according to the Eq. (4):

$$\text{distance} = \text{mean}\left|\frac{A-B}{A+B}\right| \tag{4}$$

In the formula, A and B represent arrays of simulated and experimental datasets, respectively. Experimental data from the computation of Pearson coefficient in the concatenated selections analysis were used. The mean lifetime of the replication focus calculated from the simulations providing the best match with the experimental data was 2.19 ± 0.12 h (Fig. 8a, b). Similarly, we simulated the UNG presence in the replication foci. In this case, the best match provided the model in which the presence of UNG in the replication focus started 0.18 ± 0.05 h after the replication onset and finished 0.68 ± 0.05 h before replication end. The chance of the occurrence of UNG in the non-replicating replication foci was 0.23 ± 0.02. It does not automatically mean that UNG protein is depleted from the replication focus before its replication ends as this result also depends on the changes in the accessibility of the epitope for antibody. On the other hand, it clearly indicates that the signal of UNG is progressively decreased in the replication focus before the end of its replication.

## Discussion

Two main aims related to the UNG protein function were addressed in this study. The first one was focused on the changes of the nuclear UNG level during the cell cycle. The second one concerned the kinetics of UNG protein distribution with respect to the replication foci. Several studies argue for the elevation of UNG2 level on G1/S boundary and some of them also for the preservation of high UNG2 level during the majority of the S phase[2,3,6,9]. On the other hand, some data argue against it[11]. These data come from the synchronised cells of several human cell lines (e.g. HeLa, HeLa S3, and HaCaT cells). For the cell synchronisation, methods based on the double thymidine (dT) block, nocodazole, aphidicolin, serum starvation, or mitotic shake-off were used e.g.[6,9,11,13].

In our study, we used double thymidine block for the synchronisation of HepG2 and HeLa cells. To minimize the impact of the mitochondrial UNG1 protein on the results, nuclear lysates were used, and the analysis of both UNG2 and UNG1 protein content was conducted concurrently. In contrast to the previously performed studies, we calculated for every time point the fractions of cells in particular phases of the cell cycle as none of the synchronisation protocols can keep the cell synchrony for a long time at the same level. It enabled us to evaluate the level of synchrony at various times after the release of the cells from the synchronisation block and to directly address the correlation between the nuclear UNG activity/UNG2 content and the distinct cell phase fractions. The used approach clearly showed that although the double thymidine block provides relatively high level of cell synchrony immediately after the removal of the second thymidine block, this synchrony is not utter. In addition, the cell synchrony gradually decreased in time. It is not surprising as the cell population is evidently composed of cells with the various cell cycle length and different susceptibility to the elevated thymidine concentration. Moreover, cells trapped by the first thymidine block in the S phase can exhibit different cell cycle kinetics than the rest of cells. It also further emphasises the importance of the careful analysis of the cell cycle at every time point in the similar studies.

High correlation between UrE rate and UNG2 content (Pearson coefficient = 0.93685 and 0.98999869, p-value = 0.0006 and p-value < 0.001 for HepG2 and HeLa cells, respectively) and no significant correlation

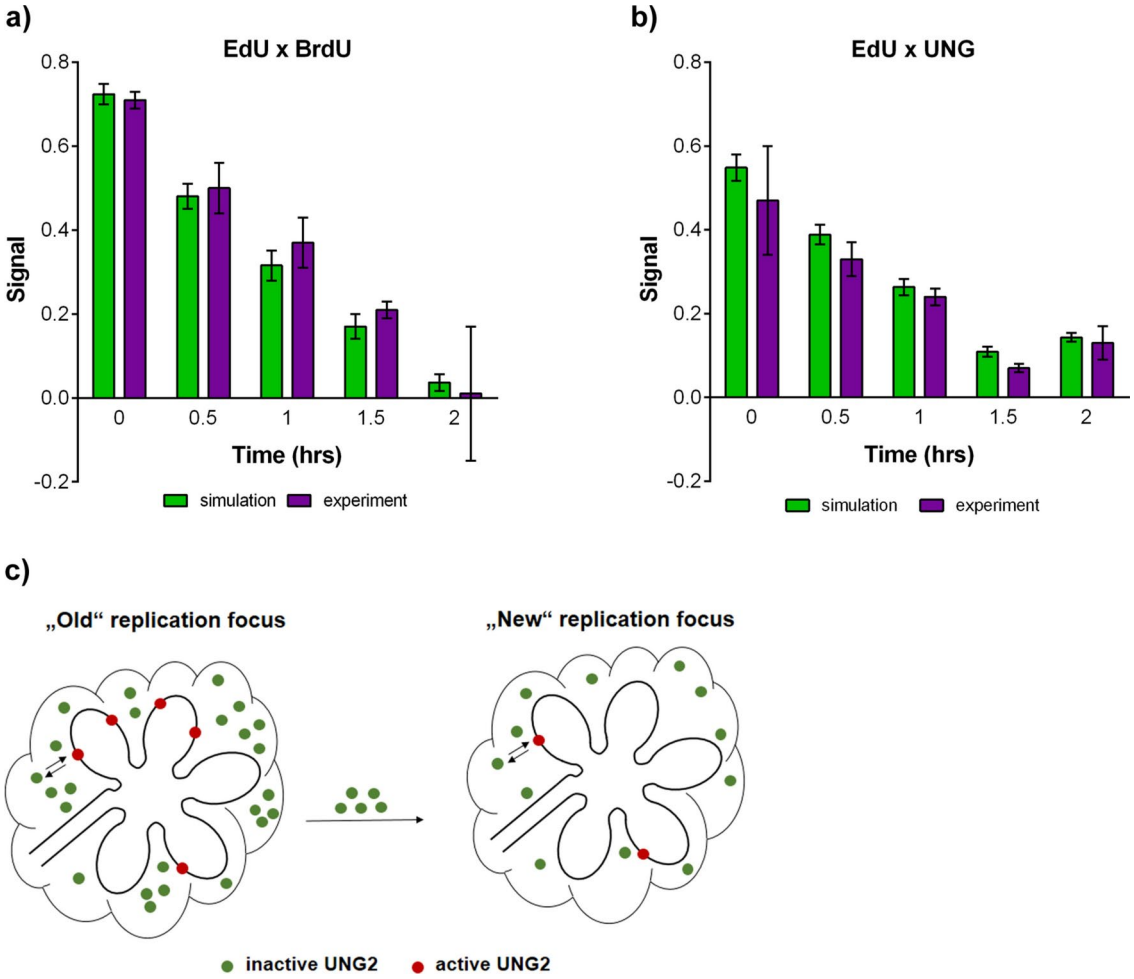


**Fig. 8**. Simulation of EdU, BrdU, and UNG labelling and the scheme of redistribution of UNG2 protein. (**a**, **b**) The ratio of the number of replication foci labelled both by EdU and BrdU or by EdU and nuclear UNG and all labelled replication foci is shown in (**a**) and (**b**), respectively. The experimental data from analysis of Pearson coefficient in the concatenated selections were used. (**c**) The scheme of redistribution of UNG2 protein from the inactive reservoir (in green) in the close proximity of replicons to the active sites on the newly replicating DNA and/or newly born replication foci (in red). The reservoir is filled by UNG2 shortly after initiation of replication in replication focus and depleted before end of focus replication.

between UrE rate and UNG1 content in the analysed time points indicated that the absolute majority of nuclear uracil excision is mediated by UNG2. This is in complete agreement with the previous finding that UNG2 is the major rate-limiting factor in repair of U:A and U:G in nuclear DNA in human cell lines[7]. On the other hand, we observed clear differences between the first and second cell cycle after the removal of the dT block. No such profound differences were observed in the control experiment if CDD levels were analysed. It indicated that the UNG2 expression is more susceptible to the dT block than the CDD expression. This susceptibility also disables to make any conclusion about the nuclear UNG activity/UNG2 content during the cell cycle. Although some aspects of the course of the UNG2 level and nuclear UNG activity indicated that both values positively correlate with the amount of the cells in the S phase, these evidences were statistically weak. As similar statistical evaluation was not available in the previous studies focused on the changes of UNG2 level/nuclear UNG activity during the cell cycle, it disabled the direct comparison with the obtained data. On the other hand, our results indicate that the dT block is not suitable approach for UNG2 studies.

The mechanism of the induction of cell synchrony by thymidine is based on the inhibition of reduction of CDP to dCDP[22]. It results into trapping a relatively high proportion of cells in the S phase. The cells encounter the consequences of the replication stress as their replication forks are stalled. It can result in the formation of single stranded DNA (ssDNA)[34]. If stalled forks are not stabilized, or if they persist for an extended period, replication forks will collapse. This collapse can result in the formation of double-stranded DNA breaks[34]. Therefore, it is not bewildering that such changes can consequently also result into changes of the timing of nuclear UNG activity in cell cycle. Although this effect could be overcome by the use of more convenient synchronisation protocol, most protocols result into changes of cell metabolism as well and therefore its choice is difficult. For example, the most frequently used alternative protocols convenient for cell synchronisation on the G1/S border include approaches based on hydroxyurea or aphidicolin[22]. However, also in this case unwanted metabolic changes were

reported. The exposure of cells to hydroxyurea or aphidicolin at concentrations commonly used to synchronise cell populations led to the phosphorylation of histone H2AX on Ser139 (induction of γH2AX) through the activation of ATM and ATR protein kinases[35–37] or DNA damage[38]. In addition, the growth imbalance and imbalances in the expression of cell cycle regulatory proteins such as cyclins B1, A, and E were reported if aphidicolin was used to synchronise cells[39].

Various effects on the cell metabolism using other synchronisation protocols based on inhibition of mitotic spindle formation[40,41], or on the use of lovastatin[42], or mimosine[43], or RO-3306[20] were described as well[22]. In addition, according to our result, although synchronisation of cells with RO-3306 led to the increased number of G2-cells, it did not lead to the decrease of the number of replicating cells. The use of the mitotic shake-off[44] can provide the possibility to overcome the use of chemicals, however, it is relatively tricky, the yield of synchronised cells is low[22], and as the synchrony is gradually lost in time, it is most suitable for the analysis of changes during G1 phase.

To overcome the unwanted effects of the synchronisation protocol, we developed a method based on the cell line with the FUCCI construct, cell sorting, and computational approach. The used approach clearly showed that the highest level of nuclear UNG activity exhibit S-phase cells. The method is relatively fast and easy to perform as it requires only three different fractions of cells to compute the relative UrE rate in the distinct cell cycle phases (see Fig. 2a).

The obtained results were in complete agreement with the immunocytochemical analysis of nuclear UNG distribution in four non-synchronized cell lines (HepG2, HeLa, hTERT RPE-1, and IMR-90 cells). This analysis also clearly showed that the signal obtained by immunocytochemical detection of nuclear UNG protein positively correlates with the replication signal in all cell lines used. It indicated that the increase in the replication activity usually positively correlates with the increase of nuclear UNG content in human cell lines. This finding was further supported by the data from experiments focused on the analysis of UrE rate after the targeted decrease of replication activity in primary cell lines using contact inhibition or in transformed cells by the senescence induction. Providing that the tested cell lines represented random sample of human cell lines, the obtained data indicates that the positive correlation between the replication activity and nuclear UNG activity/UNG content is general phenomenon of human cell lines ($p$-value = 0.004).

We also addressed the kinetics changes in the distribution of nuclear UNG in replication foci. Although the presence of UNG2 was previously documented in replication foci of HaCaT cells[13] and other studies showed that the UNG2 protein co-localizes with the PCNA protein in HeLa and U2-OS cells[9,33], the kinetics of nuclear UNG distribution in replication foci is not known. Replication foci corresponds to the clusters of simultaneously replicated adjacent replicons[45]. The estimation of the replication foci lifetime depends clearly on the model and the method used. While 45–60 min was suggested for V79 Chinese hamster cells[46], 30 min to 3 h was supposed in C2C12 mouse myoblast cells[47].

In this respect, we used three independent methods to analyse the separation of EdU and BrdU signals in the pulse-chase-pulse experiments with HeLa cells. Our results showed that 2-h chase resulted in the complete separation of the two signals. It indicates that the maximal lifetime of replication foci in HeLa cells is around 2 h. It is in agreement with our previous electron microscopy data showing that the complete separation of the biotin-labelled domains in HeLa cells occurs after 2 h and their number is quadrupled during mitosis[16]. This conclusion is also supported by our in silico experiments. The best match with the experimental data provided the simulation supposing the mean focus lifetime around 2.2 h.

Independently of the replication focus lifetime, our pulse-chase experiments with EdU and nuclear UNG mapping revealed for the first time that the complete separation of EdU and UNG signals precedes the separation of EdU and BrdU signals. It does not mean that the UNG activity is decreased at replication foci because we cannot exclude the possibility that the mapping experiments reveal non-active accumulations of this protein in the close proximity of replication activity (see Fig. 8c). As there are no data, that UNG2 is crucial only for the initial phase of replication, it can reflect the presence of a very high concentration of inactive UNG2 in replication foci, while only a very low portion of UNG2 is active. This mechanism, together with cell cycle-dependent fluctuations in UNG2 levels, can contribute to the regulation of UNG2 accessibility and activity.

In summary, our data indicate that (1) the synchronisation method based on the use of double thymidine block is not convenient for studies focused on the uracil DNA glycosylase UNG2, (2) the increase of the UrE rate in S-phase cells is a common feature of the most of the mammalian cell lines, (3) the increase of the UrE rate is accompanied by the increase of nuclear UNG content and its presence in replication foci, (4) the distribution of the nuclear UNG protein in replication foci is changed during the lifetime of the replication focus, (5) the novel developed and tested method used for the analysis of UrE rate during cell cycle can serve as a valuable tool for studies focused on the cell cycle distribution of various cellular activities/components.

## Materials and methods

### Measurement of uracil excision rate

To measure the uracil excision rate, we used assay based on the fluorescently labelled oligonucleotides described in[4]. At the beginning, m-sensors were prepared. The biotinylated anchoring oligonucleotide was coupled to the streptavidin-coated magnetic particles followed by the hybridisation with the complementary oligonucleotide (Table 3; for details of the m-sensors' preparation see[4]). We prepared m-sensors containing either uracil, thymidine (control m-sensors), or BrdU in the double-stranded oligonucleotide. Then, one volume of the prepared m-sensors with anchored double-stranded oligonucleotide probes was added to the 100 volumes of NaCa buffer (2 mM $CaCl_2$, 50 mM NaCl, 10 mM Tris–HCl, pH 7.5, and 1 mM EDTA). After magnetic separation, m-sensors were washed two times in the NaCa buffer. For magnetic separation, we used the UniTrap magnetic separator (https://imtm.cz/technologies/magnetic-unitrap).

After the last buffer change, the pellet of m-sensors was resuspended by pipetting in NaCa buffer. For UrE rate measurement, 50 µl of the prepared m-sensors (~ 0.5 µg of magnetic particles), either with uridine, or thymidine, or BrdU, was added per well of the black 384-well plate. As a blank, the NaCa buffer was used. Subsequently, 50 µl of the prepared nuclear lysates with the final protein concentration of 2 µg/ml, unless otherwise stated, was added per well of the black 384-well plate. Fluorescence was measured using the plate reader at 2-min intervals, either in 12 cycles (26 min in total) or 15 cycles (32 min in total), unless otherwise stated. Before measurement, the well plate was tempered in the plate reader to 25 °C for 4 min. We performed the analysis in four technical and three biological replicates. To evaluate the UrE rate, at first the four technical replicates were averaged and the background was subtracted from the obtained average values. Finally, the signal from m-sensors with thymidine was subtracted from the signal from the m-sensors with uracil or BrdU. The rate of the signal growth was determined as a value of a first derivation of the regression function of the dependence of the signal measured for 6-FAM at the beginning of the reaction[4].

## Cell cultures, cell synchronisation, and BrdU labelling

Human cancer cells HeLa (cervix, adenocarcinoma;[4,48]), NCI-H2009 (lung, adenocarcinoma;[49]), HCT116 (colon, colorectal carcinoma;[50,51]), U2-OS (bone, osteosarcoma;[48]), and MRC-5 cells (diploid fibroblasts, lung;[49]) all cells were a gift from Dr Marián Hajdúch, Institute of Molecular and Translational Medicine, Olomouc), IMR-90 (diploid fibroblasts, lung, ATCC, CCL-186); HeLa FUCCI (cervix, adenocarcinoma with stably expressing FUCCI construct, a gift from Dr Martin Mistrík, Institute of Molecular and Translational Medicine, Olomouc;[52,53]); HepG2 (liver, hepatocellular carcinoma;[54]), non-cancer hTERT RPE-1 (diploid, pigmented epithelium; retina hTERT-immortalized), and WI-38 (diploid, lung fibroblasts, latter three cell lines were a gift from Dr David Staněk, Institute of Molecular Genetics CAS, Prague) were used in the study.

The HeLa, HeLa FUCCI, NCI-H2009, and hTERT RPE-1 cells were cultivated in Dulbecco's modified Eagle's medium (DMEM) supplemented with 10% foetal bovine serum, 3.7 g/l of sodium bicarbonate, and 50 µg/ml of gentamicin. HepG2, IMR-90, WI-38, and MRC-5 cells were cultivated in Eagle's minimum essential medium (EMEM) supplemented with 20% foetal bovine serum, 3.7 g/l of sodium bicarbonate, and 50 µg/ml of gentamicin. HCT116 and U2-OS cells were cultivated in McCoy's culture medium supplemented with 10% foetal bovine serum, 3.7 g/l of sodium bicarbonate, and 50 µg/ml of gentamicin. The cells were cultivated at 37 °C in a humidified atmosphere containing 5% $CO_2$. All cell lines were regularly tested for mycoplasma contamination by PCR and enzymatic detection[55].

For cell synchronisation at the G1/S border, we used a double thymidine block with 2'-deoxythymidine (Sigma Aldrich)[14,16]). Briefly, HepG2 or HeLa cells were incubated with 3 mM 2'-deoxythymidine for 16 h. Thereafter, cells were released from the thymidine block by incubation in fresh medium for 12 h, followed by the second thymidine block (16 h.). After the release from the second thymidine block, the cells were incubated in a fresh culture medium for 2, 4, 8, 12, 16, 20, or 24 h.

For G2 synchronisation, protocol with RO-3306 inhibitor was used[20,21]. HepG2 and HeLa cells were incubated with 10 µM RO-3306 for 24 h.

Thereafter, nuclear lysates were prepared, or cells were labelled with BrdU for 30 min and subsequently processed for fluorescence microscopy. In the case of contact inhibition, cells were seeded to the Petri dishes (10 cm in diameter) and cultivated for at least 7 days. Contact inhibition was monitored by the bright field microscope Olympus CKX31.

## Analysis of deaminase activity by LC–MS

The CDD activity was measured using LC–MS according to[56]. Briefly, the prepared cell lysates from HepG2 and HeLa cells were thawed on ice prior to their incubation with 10 µM cytidine. To measure CDD activity, the lysates of control samples and from seven time points (for more details, see the previous chapter about cell synchronisation) were incubated in triplicate. These lysates were diluted to a uniform concentration of total protein (50 µg/ml) with the cold buffer (10 mM Tris–HCl, pH 7.4 and 10 mM KCl) and a substrate to a final volume of 70 µl. The reaction was started by adding the substrate. The mixture was stirred, 30 µl of sample immediately taken and mixed with 120 µl of cold methanol (− 80 °C) to stop the reaction. The samples were shaken at 37 °C. After 10 min, 30 µl of sample was mixed with 120 µl of cold methanol. For sufficient protein precipitation, the samples were placed at − 80 °C overnight. The samples were subsequently centrifuged (12 000 × g, 0 °C) for 20 min and 100 µl of supernatant used for LC–MS analysis. A ten-point calibration of analytical standards was prepared by binary dilution series and analysed with the batch. The upper limit of quantification (ULOQ) for cytidine and uridine was 2 µmol/l[56]. The CDD activity was calculated as the increase of uridine concentration after administration of the cytidine substrate according to the following formula (5):

$$\text{activity} = \frac{c_2 - c_0}{t} \tag{5}$$

In this formula, $c_2$ is a concentration of uridine after 10-min incubation, $c_0$ is a concentration of uridine at the beginning of the reaction, and $t$ is time of incubation (10 min).

## Induction of senescence

To study the uracil excision rate in senescent cancer cells, senescence was induced in HeLa cells by a 6-day incubation with 60 µM BrdU, in NCI-H2009 cells by a 8-day incubation with 100 µM BrdU, and in HCT116, and U2-OS cells by a 4-day incubation with 100 µM BrdU. Cellular senescence was monitored by senescence-associated β-galactosidase (SA-gal) assay, DAPI staining, and analysis of DNA replication using EdU. SA-gal staining was performed using a senescence detection kit according to the manufacturer's protocol (Abcam,

ab65351). In the case of EdU, senescent cells and control cells were washed with the fresh culture medium, incubated in it for 1 h and then incubated with 10 μM EdU for an additional hour. Subsequently, the cells were processed for fluorescence microscopy.

### Preparation of cell lysates, measurement of protein content

Cell lysates were prepared as described in[4]. Briefly, the cells plated on the Petri dish (100 mm in diameter, 70–80% confluence) were washed with 1 × PBS buffer and then quickly rinsed with the ice-cold buffer composed of 10 mM Tris–HCl, pH 7.5, and 10 mM KCl (buffer A). Thereafter, the ice-cold buffer B, composed of 10 mM Tris–HCl, pH 7.5, 10 mM KCl, 0.5 mM EDTA, and protease inhibitors (Merck), was added and the cells were incubated on ice for 20 min. The cells were scratched, using the cell scraper, transferred to the ice-cold Dounce homogeniser and homogenised (30 times). The homogenate was transferred into a 2-ml tube and centrifuged for 10 min. at 12 000 × g, 4 °C. The liquid cytoplasmic fraction was removed and used for analysis of CDD activity. Next, 50 μl of buffer B was added to the pellet, the pellet was re-suspended; 200 μl of buffer C (0.5 M KCl, 10 mM Tris–HCl, pH 7.5, 0.5 mM EDTA, and protease inhibitors) was added, samples were mixed on a laboratory vortex and incubated on ice for 40 min. The samples were briefly mixed every 10 min. After incubation, samples were centrifuged 20 min. at 12 000 × g, 4 °C. The supernatant (nuclear fraction) was transferred to the new ice-cold tube and either used for measurements or aliquoted and stored at −80 °C. Nuclear lysates were prepared from at least three independent experiments.

In the case of FACS-sorted samples, cells were centrifuged for 5 min at 50 × g and two times washed with PBS, before buffer B addition.

The protein concentrations were determined using Pierce BCA protein assay kit (ThermoFisher Scientific) according to the manufacturer's protocol.

### SDS-PAGE, western blot

The SDS-PAGE and Western blots were performed according to[4,48]. Briefly, 1 or 2 μg of the total protein was resolved by SDS-PAGE at a constant voltage of 100 V for the first 10 min. and 120 V for 1 h and 50 min, unless otherwise. The proteins were then transferred to a nitrocellulose membrane (0.2 μm pore size, Bio-Rad) using the TE 22 Mighty Small Transfer Tank (Hoefer). The staining with Ponceau S was used as a loading control[57] and the images of Ponceau S staining were collected by the ChemiDoc MP Documentation system (Bio-Rad). After washing, the membrane was blocked in 5% BSA in TBS/T (Tris-buffered saline with 0.1% Tween-20) for 1 h and incubated with primary antibody against UNG (clone OTI2C12, OriGene, TA503563) or CDD (Santa Cruz Biotechnology, sc-365292) in 5% BSA and TBS/T overnight at 4 °C with agitation. Thereafter, the membranes were washed with TBS/T and incubated with peroxidase-labelled secondary antibody. After washing, the membranes were incubated briefly with Luminata Forte peroxidase substrate (Merck). The chemiluminescence was collected by the Odyssey system (Li-Cor). The data were evaluated using ImageJ and Microsoft Excel software[4,48,58].

### BrdU, EdU, and nuclear UNG detection, DAPI staining

In the case of the detection of DNA replication by fluorescence microscopy, the cells grown on coverslips (12 mm in diameter) labelled either with BrdU or EdU were fixed with ice-cold 70% ethanol (1 h, −20 °C) or 2% formaldehyde in 1 × PBS (10 min, room temperature, RT). For the detection of incorporated BrdU and EdU, the protocols described in[52,53] were used. For the simultaneous detection of EdU and UNG2 protein, fixation with 2% formaldehyde in 1 × PBS (10 min, RT) was used. After brief washing in TrisNa buffer (25 mM Tris–HCl, pH 7.5 and 150 mM NaCl), cells were permeabilised in 0.2% Triton X-100 in 1 × PBS (10 min, RT). Then, UNG protein was detected using anti-UNG antibody in TrisNa buffer (1:100, 1 h, RT). After washing with TrisNa buffer, cells were incubated with anti-mouse antibody conjugated with AlexaFluor 488 in TrisNa buffer (1:100, 1 h, RT). Cells were briefly washed with TrisNa buffer followed by washing in 1 × PBS buffer and incubated with 2% formaldehyde in PBS (10 min, RT). After washing in 1 × PBS, EdU was detected by click reaction as described in[53].

In the case of samples from FACS, the CytoTrap apparatus and protocol described in Ligasová et al., 2021 was used for EdU detection[59]. In all cases, samples were concurrently counterstained with 10 μM DAPI in TrisNa buffer for 30 min at room temperature (RT)[59]. The samples were analysed using fluorescence microscopy and image cytometry.

### FACS sorting of HeLa FUCCI cells

HeLa FUCCI cells were collected, resuspended in growth medium and cell suspension density was adjusted to a final concentration of $10 \times 10^6$ cells/ml. Cells were analysed by FACSAria II (Becton Dickinson) cell sorter. First of all, 50 000 cells were acquired to set gating. Dead cells and debris were gated out by forward scatter versus side scatter gating. Then, intact cells were gated and brought to red/green channels dot-plot diagram. Gating strategy used to sort HeLa FUCCI cells into three clusters representing three distinct phases of the cell cycle was based on distinguishing the cells expressing the red tag (Cdt1, G1) from the cells expressing the green tag (geminin, S and G2/M). Cells expressing both markers simultaneously, marking the S phase, were clustered in a third group. Both green and red fluorescent markers were excited by a 488 nm argon laser line and fluorescence signals were collected at 530 nm (green) and 575 nm (red) channels. Cells corresponding to distinct cell cycle phases based on their fluorescence status were collected to FACS tubes at 4 °C by 4-way sorting mode setting. At least $4 \times 10^6$ cells were collected for each cell-cycle-phase fraction. The tubes were immediately put on ice and proceeded as described elsewhere.

## Data acquisition, computational approach, and data evaluation

When the fluorescence signal was measured in black 384-well plates (UrE rate assay), the Infinite 200 Pro Plate Reader (Tecan) was used. The fluorescence of 6-FAM was measured at 488 nm excitation wavelength and 520 nm emission wavelength. The signal was measured every 2 min in 12 or 15 cycles, unless otherwise stated. Before each measurement, the samples were shaken by the plate reader (10 s, 1.5 mm amplitude)[4].

When fluorescence microscopy was used, all images were acquired using an Olympus IX83 microscope (UPLFLN 2PH objective 10×, NA 0.3, LUCPLFLN PH objective 40×, NA 0.6, or UPLSAPO O 100×, NA 1.40), equipped with a Zyla camera (Andor) with a resolution of 1 024 × 1 024 or 2 048 × 2 048 pixels using acquisition software (Olympus cellSense Dimension 2.3, Olympus)[4,55].

The data concerning the cell cycle analysis and DNA replication signal were analysed using ilastik 1.3.3post3 (https://www.ilastik.org/)[60], CellProfiler 4.2.1 (https://cellprofiler.org/)[61,62], Image J[63], and Microsoft Excel software. In average, 15 000 cells were evaluated for every sample. The final graphs were done in GraphPad Prism 6.

The system of equations was solved, and descriptive statistics of solutions were calculated using Python 3.8[64], NumPy[65], and Pandas[66] libraries. The Pearson coefficients and p-values were calculated using the SciPy library[67], GraphPad Prism 6, and SIMCIM tools. PNA ratios were calculated using SIMCIM tools software (available from https://privatecloud.imtm.cz/s/QkidNLM473GSmF4). In silico analysis was performed using Python, Numpy, and Pandas libraries. Shapiro–Wilk test of normality, Pearson correlation, and Mann–Whitney test were computed using SciPy library[67] and SIMCIM tools. The value of the chance that the 5 different human cell lines contain the highest content of UNG2 in S phase as a result of a random choice was calculated as one to fifth power of 3 as there is fifth power of three of all solutions and only one solution provided result where S phase exhibits highest signal in all cases. For the computation of the statistical significance tests of independent correlation coefficients the Python script based on the Fisher Z-Transformation was used (https://github.com/psinger/CorrelationStats/blob/master/corrstats.py). Adobe Photoshop was used to prepare the final figures. All experiments were conducted in three independent replicates. The data are presented as the mean values ± standard deviation.

## Data availability

All data are included in this article (and its electronic supplementary material files). Additional data supporting the findings are available from the corresponding authors upon reasonable request. The Python codes are available upon request. The SIMCIM tools software can be downloaded from https://privatecloud.imtm.cz/s/QkidNLM473GSmF4.

Received: 14 October 2024; Accepted: 23 December 2024
Published online: 24 January 2025

## References

1. Pan, M. R., Li, K., Lin, S. Y. & Hung, W. C. Connecting the dots: From DNA damage and repair to aging. *Int. J. Mol. Sci.* **17**, 685. https://doi.org/10.3390/ijms17050685 (2016).
2. Mjelle, R. et al. Cell cycle regulation of human DNA repair and chromatin remodeling genes. *DNA Repair (Amst)* **30**, 53–67. https://doi.org/10.1016/j.dnarep.2015.03.007 (2015).
3. Krokan, H. E. & Bjoras, M. Base excision repair. *Cold Spring Harb. Perspect. Biol.* **5**, a012583. https://doi.org/10.1101/cshperspect.a012583 (2013).
4. Ligasova, A., Rosenberg, I., Bockova, M., Homola, J. & Koberna, K. Anchored linear oligonucleotides: The effective tool for the real-time measurement of uracil DNA glycosylase activity. *Open Biol.* **11**, 210136. https://doi.org/10.1098/rsob.210136 (2021).
5. Kavli, B. et al. hUNG2 is the major repair enzyme for removal of uracil from U: A matches, U: G mismatches, and U in single-stranded DNA, with hSMUG1 as a broad specificity backup. *J. Biol. Chem.* **277**, 39926–39936. https://doi.org/10.1074/jbc.M207107200 (2002).
6. Hardeland, U., Kunz, C., Focke, F., Szadkowski, M. & Schar, P. Cell cycle regulation as a mechanism for functional separation of the apparently redundant uracil DNA glycosylases TDG and UNG2. *Nucleic Acids Res.* **35**, 3859–3867. https://doi.org/10.1093/nar/gkm337 (2007).
7. Visnes, T., Akbari, M., Hagen, L., Slupphaug, G. & Krokan, H. E. The rate of base excision repair of uracil is controlled by the initiating glycosylase. *DNA Repair (Amst.)* **7**, 1869–1881. https://doi.org/10.1016/j.dnarep.2008.07.012 (2008).
8. Hardeland, U. et al. Thymine DNA glycosylase. *Prog. Nucleic Acid Res. Mol. Biol.* **68**, 235–253. https://doi.org/10.1016/s0079-6603(01)68103-0 (2001).
9. Hagen, L. et al. Cell cycle-specific UNG2 phosphorylations regulate protein turnover, activity and association with RPA. *EMBO J.* **27**, 51–61. https://doi.org/10.1038/sj.emboj.7601958 (2008).
10. Haug, T. et al. Regulation of expression of nuclear and mitochondrial forms of human uracil-DNA glycosylase. *Nucleic Acids Res.* **26**, 1449–1457. https://doi.org/10.1093/nar/26.6.1449 (1998).
11. Fischer, J. A. & Caradonna, S. J. Analysis of nuclear uracil DNA-glycosylase (nUDG) turnover during the cell cycle. *Methods Mol. Biol.* **1524**, 177–188. https://doi.org/10.1007/978-1-4939-6603-5_11 (2017).
12. Fischer, J. A., Muller-Weeks, S. & Caradonna, S. Proteolytic degradation of the nuclear isoform of uracil-DNA glycosylase occurs during the S phase of the cell cycle. *DNA Repair (Amst)* **3**, 505–513. https://doi.org/10.1016/j.dnarep.2004.01.012 (2004).
13. Otterlei, M. et al. Post-replicative base excision repair in replication foci. *EMBO J.* **18**, 3834–3844. https://doi.org/10.1093/emboj/18.13.3834 (1999).
14. Koberna, K. et al. Electron microscopy of DNA replication in 3-D: Evidence for similar-sized replication foci throughout S-phase. *J. Cell Biochem.* **94**, 126–138. https://doi.org/10.1002/jcb.20300 (2005).
15. Ligasova, A. & Koberna, K. The organisation of replisomes. *DNA Replication—Current Advances*, 253–268, Book_https://doi.org/10.5772/791 (2011).
16. Ligasova, A., Raska, I. & Koberna, K. Organization of human replicon: Singles or zipping couples?. *J. Struct. Biol.* **165**, 204–213. https://doi.org/10.1016/j.jsb.2008.11.004 (2009).
17. Sarno, A. et al. Uracil-DNA glycosylase UNG1 isoform variant supports class switch recombination and repairs nuclear genomic uracil. *Nucleic Acids Res.* **47**, 4569–4585. https://doi.org/10.1093/nar/gkz145 (2019).
18. Hayran, A. B. et al. RPA guides UNG to uracil in ssDNA to facilitate antibody class switching and repair of mutagenic uracil at the replication fork. *Nucleic Acids Res.* **52**, 784–800. https://doi.org/10.1093/nar/gkad1115 (2024).

19. Micozzi, D. et al. Human cytidine deaminase: A biochemical characterization of its naturally occurring variants. *Int. J. Biol. Macromol.* **63**, 64–74. https://doi.org/10.1016/j.ijbiomac.2013.10.029 (2014).
20. Vassilev, L. T. Cell cycle synchronization at the G2/M phase border by reversible inhibition of CDK1. *Cell Cycle* **5**, 2555–2556. https://doi.org/10.4161/cc.5.22.3463 (2006).
21. Vassilev, L. T. et al. Selective small-molecule inhibitor reveals critical mitotic functions of human CDK1. *Proc. Natl. Acad. Sci. U. S. A.* **103**, 10660–10665. https://doi.org/10.1073/pnas.0600447103 (2006).
22. Ligasova, A. & Koberna, K. Strengths and weaknesses of cell synchronization protocols based on inhibition of DNA synthesis. *Int. J. Mol. Sci.* https://doi.org/10.3390/ijms221910759 (2021).
23. Sakaue-Sawano, A. et al. Visualizing spatiotemporal dynamics of multicellular cell-cycle progression. *Cell* **132**, 487–498. https://doi.org/10.1016/j.cell.2007.12.033 (2008).
24. Kaida, A. & Miura, M. Differential dependence on oxygen tension during the maturation process between monomeric Kusabira Orange 2 and monomeric Azami Green expressed in HeLa cells. *Biochem. Biophys. Res. Commun.* **421**, 855–859. https://doi.org/10.1016/j.bbrc.2012.04.102 (2012).
25. McGarry, T. J. & Kirschner, M. W. Geminin, an inhibitor of DNA replication, is degraded during mitosis. *Cell* **93**, 1043–1053. https://doi.org/10.1016/S0092-8674(00)81209-X (1998).
26. Nishitani, H., Lygerou, Z. & Nishimoto, T. Proteolysis of DNA replication licensing factor Cdt1 in S-phase is performed independently of Geminin through its N-terminal region. *J. Biol. Chem.* **279**, 30807–30816. https://doi.org/10.1074/jbc.M312644200 (2004).
27. Yoshida, K. & Inoue, I. Regulation of Geminin and Cdt1 expression by E2F transcription factors. *Oncogene* **23**, 3802–3812. https://doi.org/10.1038/sj.onc.1207488 (2004).
28. Zielke, N. & Edgar, B. A. FUCCI sensors: Powerful new tools for analysis of cell proliferation. *Wiley Interdiscip. Rev. Dev. Biol.* **4**, 469–487. https://doi.org/10.1002/wdev.189 (2015).
29. Seluanov, A. et al. Hypersensitivity to contact inhibition provides a clue to cancer resistance of naked mole-rat. *Proc. Natl. Acad. Sci. U. S. A.* **106**, 19352–19357. https://doi.org/10.1073/pnas.0905252106 (2009).
30. Petrova, N. V., Velichko, A. K., Razin, S. V. & Kantidze, O. L. Small molecule compounds that induce cellular senescence. *Aging Cell* **15**, 999–1017. https://doi.org/10.1111/acel.12518 (2016).
31. Gonzalez-Gualda, E., Baker, A. G., Fruk, L. & Munoz-Espin, D. A guide to assessing cellular senescence in vitro and in vivo. *FEBS J.* **288**, 56–80. https://doi.org/10.1111/febs.15570 (2021).
32. Kudlova, N., De Sanctis, J. B. & Hajduch, M. Cellular senescence: Molecular targets, biomarkers, and senolytic drugs. *Int. J. Mol. Sci.* https://doi.org/10.3390/ijms23084168 (2022).
33. Torseth, K. et al. The UNG2 Arg88Cys variant abrogates RPA-mediated recruitment of UNG2 to single-stranded DNA. *DNA Repair* **11**, 559–569. https://doi.org/10.1016/j.dnarep.2012.03.006 (2012).
34. Zeman, M. K. & Cimprich, K. A. Causes and consequences of replication stress. *Nat. Cell Biol.* **16**, 2–9. https://doi.org/10.1038/ncb2897 (2014).
35. Darzynkiewicz, Z., Halicka, H. D., Zhao, H. & Podhorecka, M. Cell synchronization by inhibitors of DNA replication induces replication stress and DNA damage response: Analysis by flow cytometry. *Methods Mol. Biol.* **761**, 85–96. https://doi.org/10.1007/978-1-61779-182-6_6 (2011).
36. Halicka, D. et al. DNA damage response resulting from replication stress induced by synchronization of cells by inhibitors of DNA replication: Analysis by flow cytometry. *Methods Mol. Biol.* **1524**, 107–119. https://doi.org/10.1007/978-1-4939-6603-5_7 (2017).
37. Kurose, A., Tanaka, T., Huang, X., Traganos, F. & Darzynkiewicz, Z. Synchronization in the cell cycle by inhibitors of DNA replication induces histone H2AX phosphorylation: An indication of DNA damage. *Cell Prolif.* **39**, 231–240. https://doi.org/10.1111/j.1365-2184.2006.00380.x (2006).
38. Hammond, E. M., Green, S. L. & Giaccia, A. J. Comparison of hypoxia-induced replication arrest with hydroxyurea and aphidicolin-induced arrest. *Mutat. Res.* **532**, 205–213. https://doi.org/10.1016/j.mrfmmm.2003.08.017 (2003).
39. Gong, J., Traganos, F. & Darzynkiewicz, Z. Growth imbalance and altered expression of cyclins B1, A, E, and D3 in MOLT-4 cells synchronized in the cell cycle by inhibitors of DNA replication. *Cell Growth Differ.* **6**, 1485–1493 (1995).
40. De Brabander, M. J., Van de Veire, R. M., Aerts, F. E., Borgers, M. & Janssen, P. A. The effects of methyl (5-(2-thienylcarbonyl)-1H-benzimidazol-2-yl) carbamate, (R 17934; NSC 238159), a new synthetic antitumoral drug interfering with microtubules, on mammalian cells cultured in vitro. *Cancer Res.* **36**, 905–916 (1976).
41. Salmon, E. D., McKeel, M. & Hays, T. Rapid rate of tubulin dissociation from microtubules in the mitotic spindle in vivo measured by blocking polymerization with colchicine. *J. Cell Biol.* **99**, 1066–1075. https://doi.org/10.1083/jcb.99.3.1066 (1984).
42. Javanmoghadam-Kamrani, S. & Keyomarsi, K. Synchronization of the cell cycle using lovastatin. *Cell Cycle* **7**, 2434–2440. https://doi.org/10.4161/cc.6364 (2008).
43. Park, S. Y. et al. Mimosine arrests the cell cycle prior to the onset of DNA replication by preventing the binding of human Ctf4/And-1 to chromatin via Hif-1alpha activation in HeLa cells. *Cell Cycle* **11**, 761–766. https://doi.org/10.4161/cc.11.4.19209 (2012).
44. Zwanenburg, T. S. Standardized shake-off to synchronize cultured CHO cells. *Mutat Res.* **120**, 151–159. https://doi.org/10.1016/0165-7992(83)90157-4 (1983).
45. Nakamura, H., Morita, T. & Sato, C. Structural organizations of replicon domains during DNA synthetic phase in the mammalian nucleus. *Exp. Cell Res.* **165**, 291–297. https://doi.org/10.1016/0014-4827(86)90583-5 (1986).
46. Manders, E. M., Stap, J., Brakenhoff, G. J., van Driel, R. & Aten, J. A. Dynamics of three-dimensional replication patterns during the S-phase, analysed by double labelling of DNA and confocal microscopy. *J. Cell Sci.* **103**(Pt 3), 857–862. https://doi.org/10.1242/jcs.103.3.857 (1992).
47. Leonhardt, H. et al. Dynamics of DNA replication factories in living cells. *J. Cell Biol.* **149**, 271–280. https://doi.org/10.1083/jcb.149.2.271 (2000).
48. Ligasova, A. et al. Dr Jekyll and Mr Hyde: a strange case of 5-ethynyl-2 '-deoxyuridine and 5-ethynyl-2 '- deoxycytidine. *Open Biol.* **6**, 150172. https://doi.org/10.1098/rsob.150172 (2016).
49. Ligasova, A. & Koberna, K. Quantification of fixed adherent cells using a strong enhancer of the fluorescence of DNA dyes. *Sci. Rep.* **9**, 8701. https://doi.org/10.1038/s41598-019-45217-9 (2019).
50. Ligasova, A., Liboska, R., Rosenberg, I. & Koberna, K. The fingerprint of anti-bromodeoxyuridine antibodies and its use for the assessment of their affinity to 5-bromo-2'-deoxyuridine in cellular DNA under various conditions. *PLoS One* **10**, e0132393. https://doi.org/10.1371/journal.pone.0132393 (2015).
51. Ligasova, A., Strunin, D., Friedecky, D., Adam, T. & Koberna, K. A fatal combination: A thymidylate synthase inhibitor with DNA damaging activity. *PLoS One* **10**, e0117459. https://doi.org/10.1371/journal.pone.0117459 (2015).
52. Ligasova, A., Konecny, P., Frydrych, I. & Koberna, K. Cell cycle profiling by image and flow cytometry: The optimised protocol for the detection of replicational activity using 5-Bromo-2'-deoxyuridine, low concentration of hydrochloric acid and exonuclease III. *PLoS One* **12**, e0175880. https://doi.org/10.1371/journal.pone.0175880 (2017).
53. Ligasova, A., Konecny, P., Frydrych, I. & Koberna, K. Looking for ugly ducklings: The role of the stability of BrdU-antibody complex and the improved method of the detection of DNA replication. *PLoS One* **12**, e0174893. https://doi.org/10.1371/journal.pone.0174893 (2017).
54. Cvackova, Z. et al. Pontin is localized in nucleolar fibrillar centers. *Chromosoma* **117**, 487–497. https://doi.org/10.1007/s00412-008-0170-8 (2008).

55. Ligasova, A. et al. A new sensitive method for the detection of mycoplasmas using fluorescence microscopy. *Cells* **8**, 1510. https://doi.org/10.3390/cells8121510 (2019).
56. Ligasova, A., Pisklakova, B., Friedecky, D. & Koberna, K. A new technique for the analysis of metabolic pathways of cytidine analogues and cytidine deaminase activities in cells. *Sci. Rep.* **13**, 20530. https://doi.org/10.1038/s41598-023-47792-4 (2023).
57. Romero-Calvo, I. et al. Reversible Ponceau staining as a loading control alternative to actin in Western blots. *Anal. Biochem.* **401**, 318–320. https://doi.org/10.1016/j.ab.2010.02.036 (2010).
58. Miller, L. P. *ImageJ gel analysis*, http://www.lukemiller.org/ImageJ_gel_analysis.pdf (2010).
59. Ligasova, A. & Koberna, K. New Concept and Apparatus for Cytocentrifugation and Cell Processing for Microscopy Analysis. *Int J Mol Sci* **22**, https://doi.org/10.3390/ijms22137098 (2021).
60. Berg, S. et al. ilastik: Interactive machine learning for (bio)image analysis. *Nat. Methods* **16**, 1226–1232. https://doi.org/10.1038/s41592-019-0582-9 (2019).
61. Carpenter, A. E. et al. Cell Profiler: Image analysis software for identifying and quantifying cell phenotypes. *Genome Biol.* **7**, R100. https://doi.org/10.1186/gb-2006-7-10-r100 (2006).
62. Kamentsky, L. et al. Improved structure, function and compatibility for cell profiler: Modular high-throughput image analysis software. *Bioinformatics* **27**, 1179–1180. https://doi.org/10.1093/bioinformatics/btr095 (2011).
63. Schindelin, J. et al. Fiji: An open-source platform for biological-image analysis. *Nat. Methods* **9**, 676–682. https://doi.org/10.1038/nmeth.2019 (2012).
64. Van Rossum, G. & Drake, F. L. *Python 3 Reference Manual*. (Createspace, 2009).
65. Harris, C. R. et al. Array programming with NumPy. *Nature* **585**, 357–362. https://doi.org/10.1038/s41586-020-2649-2 (2020).
66. McKinney, W. In *Proceedings of the 9th Python in Science Conference* 51–56.
67. Virtanen, P. et al. SciPy 1.0: Fundamental algorithms for scientific computing in Python. *Nat. Methods* **17**, 261–272. https://doi.org/10.1038/s41592-019-0686-2 (2020).


## Acknowledgements

We would like to thank to Mrs. Masopustová for performing western blots.

## Author contributions

All authors contributed to the study conception and design. Conceptualization, validation, visualization and writing the original draft was made by Anna Ligasová and Karel Koberna. Data curation, formal analysis, investigation, methodology, and writing the review & editing were performed by Anna Ligasová, Ivo Frydrych, Barbora Piskláková, David Friedecký, and Karel Koberna. All authors have read and agreed to the published version of the manuscript.

## Funding

This research was funded by the Ministry of Health of the Czech Republic through the project NU22-08-00148, by the Technology Agency of the Czech Republic, grant number TN01000013, by the Ministry of Education, Youth and Sports of the Czech Republic-projects EATRIS-CZ, grant number LM2018133, EXCELES, grant number LX22NPO5102, SALVAGE, grant number CZ.02.01.01/00/22_008/0004644, and by the project BBMRI-CZ, grant number LM2023033.

## Declarations

## Competing interests

Palacký University Olomouc holds a Czech patents (CZ 307304; CZ 306187, and CZ308387) and utility models (34386 and 34442) relating to the approach for the real-time measurement of glycosylase activity. Name of inventors: A.L., K.K. The authors declare no other conflict of interest. The rest of the authors has no competing interests. The funders had no role in the design of the study; in the collection, analyses, or interpretation of data; in the writing of the manuscript, or in the decision to publish the results.

## Additional information

**Supplementary Information** The online version contains supplementary material available at https://doi.org/10.1038/s41598-024-84408-x.

**Correspondence** and requests for materials should be addressed to A.L. or K.K.